JACS
JOURNAL OF THE AMERICAN CHEMICAL SOCIETY
pubs.acs.org/JACS
Article

Cyclophane-Sustained Ultrastable Porphyrins

Wenqi Liu, Chenjian Lin, Jacob A. Weber, Charlotte L. Stern, Ryan M. Young, Michael R. Wasielewski, and J. Fraser Stoddart*

Cite This: J. Am. Chem. Soc. 2020, 142, 8938−8945
Read Online
ACCESS | Metrics & More | Article Recommendations | Supporting Information

ABSTRACT: We report the encapsulation of free-base and zinc porphyrins by a tricyclic cyclophane receptor with subnanomolar binding affinities in water. The high affinities are sustained by the hydrophobic effect and multiple [CH···π] interactions covering large [π···π] stacking surfaces between the substrate porphyrins and the receptor. We discovered two co-conformational isomers of the 1:1 complex, where the porphyrin is orientated differently inside the binding cavity of the receptor on account of its tricyclic nature. The photophysical properties and chemical reactivities of the encapsulated porphyrins are modulated to a considerable extent by the receptor. Improved fluorescence quantum yields, red-shifted absorptions and emissions, and nearly quantitative energy transfer processes highlight the emergent photophysical enhancements. The encapsulated porphyrins enjoy unprecedented chemical stabilities, where their D/H exchange, protonation, and solvolysis under extremely acidic conditions are completely blocked. We anticipate that the ultrahigh stabilities and improved optical properties of these encapsulated porphyrins will find applications in single-molecule materials, artificial photodevices, and biomedical appliances.

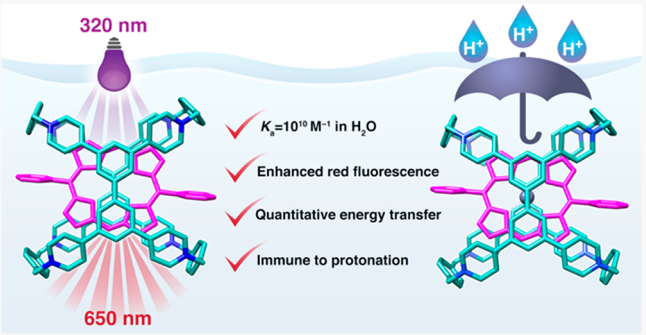

INTRODUCTION

Molecular recognition is utilized comprehensively by nature for the regulation of biological processes.[1,2] One of the goals in the supramolecular chemistry community is to make[3,4] synthetic receptors that can hold a candle to the binding affinities and functionalities of bioreceptors. In recent years, several wholly synthetic receptors have been reported[5,6] with substrate-binding affinities exceeding the performance of naturally occurring receptors. These high-affinity synthetic receptors have shown[7] promising applications in drug delivery, membrane functionalization, and protein purification. Advances in these biotechnologies create new and demanding requirements for synthetic receptors with not only high binding affinities but also integrated functionalities.[8−15] It is desirable to develop high-affinity receptors for functional substrates such as dye molecules.[16−19] Although there have been numerous reports[20−22] on dye encapsulations by several well-known receptors such as cyclodextrins, calixarenes, cucurbiturils, and pillararenes, most of them fail to encapsulate dyes at nanomolar concentrations on account of their low binding affinities. Examples of high-affinity receptors for functional dye molecules[23−27] are rare and are urgently needed[28] to meet the demanding requirement of biotechnologists and scientists working in related fields.

Porphyrins are indispensable dyes in biology and fulfill many crucial biological functions, such as oxygen transport, photosynthesis, and metabolism.[29] Most porphyrins in nature exist as noncovalent complexes and are buried deep inside the superstructures of porphyrin-binding proteins, where their microenvironments not only govern the versatile functions of porphyrins but also protect them from direct interactions with solvents and solutes.[30] Much effort has been devoted to making synthetic mimics of these porphyrin-containing devices[30−32] and engineering them to express functions in artificial photodevices,[33,34] model enzymes,[35−40] and biotechnologies.[41−43] To this end, one of our goals is to develop artificial receptors that bind strongly with porphyrins in confined microenvironments, in which we can modulate the photoelectrical properties and chemical reactivities of the encapsulated porphyrins.[4,8,44]

Binding of porphyrins has been explored using chemically modified proteins and peptides,[30,31,45] nucleotides,[46,47] and other naturally derived compounds.[48,49] Porphyrins have also been substrates for intense targeting in the supramolecular community, where cyclodextrins,[50−52] calixarenes,[53] cucurbiturils,[54,55] cyclophanes,[56,57] foldamers,[58] and coordination metal cages[39,59] have all been developed in order to interact with porphyrins with various functions in mind. Despite all these advances in mimicking porphyrin-binding proteins, the challenge remains to design a monomeric high-affinity receptor

Received: February 27, 2020
Published: April 3, 2020

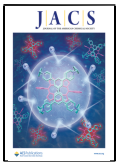

https://dx.doi.org/10.1021/jacs.0c02311
J. Am. Chem. Soc. 2020, 142, 8938−8945

that can fully encapsulate porphyrins on account of their large sizes which exceed the cavity sizes of current synthetic receptors.[57]

Recently, we designed[27] an X-shaped octacationic cyclophane, **XCage**$^{8+}$, which features a large and rigid binding cavity. The constitution of **XCage**$^{8+}$ exhibits high stereoelectronic complementarity toward perylene diimide (PDI) dyes with picomolar binding affinities in water. Low-level molecular modeling suggests that the porphyrin core is a good fit with the binding cavity of **XCage**$^{8+}$, where multiple [$\pi\cdots\pi$] and [CH$\cdots\pi$] interactions come into play upon binding. This stereoelectronic complementarity has motivated us to explore the possibility of using **XCage**$^{8+}$ as a porphyrin receptor in water. Herein, we report the encapsulation of free-base porphyrin and Zn-porphyrin using **XCage**$^{8+}$ as a receptor with subnanomolar binding affinities. These ultrahigh affinities can be attributed to multiple [CH$\cdots\pi$] interactions in addition to large [$\pi\cdots\pi$] stacking surfaces between the substrate porphyrins and the receptor **XCage**$^{8+}$. Two types of co-conformational isomers, in which the porphyrin substrates are orientated differently inside the binding cavity of **XCage**$^{8+}$, were uncovered by ^{1}H NMR spectroscopy in D_2O. The photophysical properties of the encapsulated porphyrins turn out to be modulated by **XCage**$^{8+}$. Improved fluorescence quantum yields, red-shifted absorptions and emissions, and a nearly quantitative energy transfer process are all observed. In addition to these physical attributes, the encapsulated porphyrins show remarkable chemical stabilities, reflected in the fact that their protonation, D/H exchange, and solvolysis under extremely acidic conditions are blocked.

RESULTS AND DISCUSSION

X-ray Crystallographic Analysis. X-ray crystallography was used to perform a preliminary evaluation of the porphyrin binding capability using **XCage**$^{8+}$. A mixture of the model compounds **mPorp-2H**(**Zn**) with **XCage**$^{8+}$ results (Figure 1) in

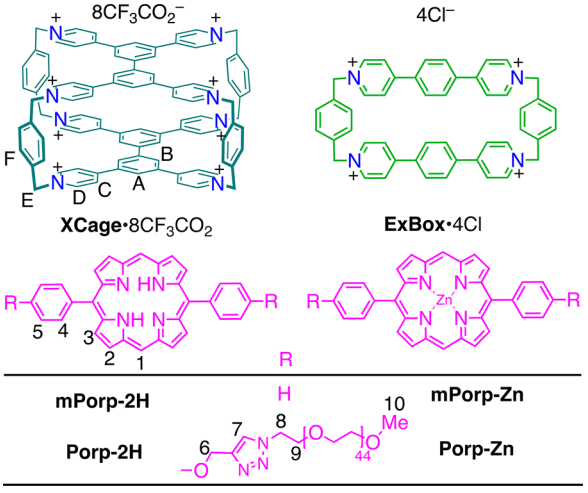

Figure 1. Structural formulas of the compounds relevant to the physical organic investigation discussed in this paper.

the solubilization of these porphyrins in water—a good indication of complex formation. Single crystals were obtained by slow diffusion of iPr_2O into Me_2CO solutions of these complexes. In the superstructures of **mPorp-2H**(**Zn**)⊂**XCage**$^{8+}$, both **mPorp-2H** and **mPorp-Zn** are positioned (Figure 2) horizontally with respect to the binding cavity of **XCage**$^{8+}$. The

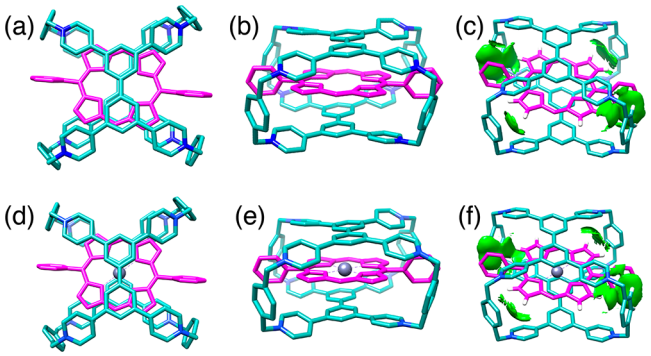

Figure 2. Stick representation of the solid-sate superstructures obtained from single-crystal X-ray crystallography. (a) Top-down view, (b) side-on view, and (c) [CH$\cdots\pi$] binding surfaces of **mPorp-2H**⊂**XCage**$^{8+}$. (d) Top-down view, (e) side-on view, and (f) [CH$\cdots\pi$] binding surfaces of **mPorp-Zn**⊂**XCage**$^{8+}$.

diphenyl roof and floor of **XCage**$^{8+}$ show large areas of [$\pi\cdots\pi$] stacking with the porphyrin cores. Furthermore, there are multiple [CH$\cdots\pi$] interactions between the four *p*-xylylene pillars of **XCage**$^{8+}$ and the porphyrin. These [CH$\cdots\pi$] distances range from 2.9 to 4.4 Å. The noncovalent bonding interactions were visualized (Figure S23) by using the independent gradient model (IGM) analysis.[60]

NMR Spectroscopy in Solution. Both **mPorp-2H** and **mPorp-Zn** are insoluble in water, preventing our ability to carry out quantitative binding studies. In order to evaluate the receptor substrate binding in solution, two water-soluble porphyrins (**Porp-2H** and **Porp-Zn**), flanked by polydispersed PEG chains, were synthesized using standard protocols. Upon mixing **XCage**$^{8+}$ with **Porp-2H**(**Zn**) in D_2O, the complexes formed quantitatively, as indicated by the ^{1}H NMR spectra. Surprisingly, two sets of proton signals for the encapsulated porphyrins are observed (Figure 3), indicating the presence of two co-conformational isomers. One set of ^{1}H NMR signals corresponds to co-conformer H as defined by X-ray crystallography. The other set of ^{1}H NMR signals most likely originates from co-conformer V in which the porphyrin substrate is located vertically in relation to the binding cavity of **XCage**$^{8+}$. The meso protons (1) of the porphyrin are obscured by **XCage**$^{8+}$ in co-conformer H, and their chemical shift appears at 8.8 ppm as a result of the shielding effects by the diphenyl units. In contrast, the meso protons (1) in co-conformer V are beyond the coverage of **XCage**$^{8+}$; thus, their chemical shift shows up at 10.1 ppm. By comparing integrations, we found that the ratios of co-conformer V to co-conformer H are 6:4 and 4:6, respectively, for **Porp-2H**⊂**XCage**$^{8+}$ and **Porp-Zn**⊂**XCage**$^{8+}$. Co-conformer V represents a kinetically trapped metastable state, which is gradually transformed into co-conformer H over time. It takes 72 h at room temperature to complete the transformation in the case of **Porp-Zn**⊂**XCage**$^{8+}$. The transformation of **Porp-2H**⊂**XCage**$^{8+}$ is more difficult to achieve and requires additional heating at 70 °C for 24 h to form co-conformer H. This observation differs from the previously reported[27] PDI ⊂ **XCage**$^{8+}$ complex, where the substrate PDI is only observed as being positioned vertically with respect to the binding cavity of **XCage**$^{8+}$. The co-existence of co-conformers H and V can be attributed to the square-shaped porphyrin core, which presents a similar overlapping surface area with **XCage**$^{8+}$ in both co-conformers. The phenyl groups in the porphyrin are expected to experience unfavorable steric strain in co-conformer V, making it a less stable species when compared with co-conformer H,

https://dx.doi.org/10.1021/jacs.0c02311
J. Am. Chem. Soc. 2020, 142, 8938−8945

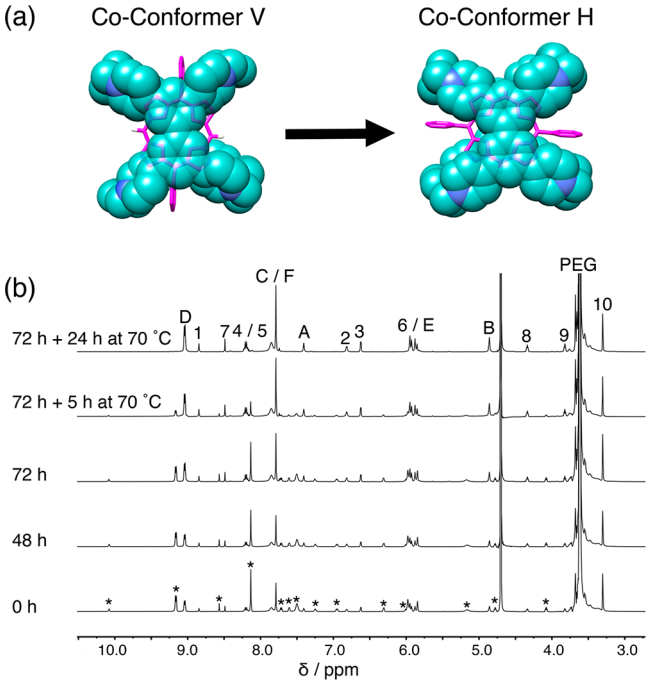

Figure 3. Co-conformational isomer transformation in D_2O solution tracked by dynamic ^1H NMR spectroscopy. (a) Molecular models illustrating the transformation of co-conformer V to H. (b) ^1H NMR (500 MHz, D_2O, 25 °C) spectra of **Porp-2H⊂XCage^{8+}** collected at 0, 48, and 72 h at room temperature, along with additional heating at 70 °C for 5 and 24 h. The asterisks (*) identify ^1H NMR signals at 0 h for the co-conformer V of **Porp-2H⊂XCage^{8+}**.

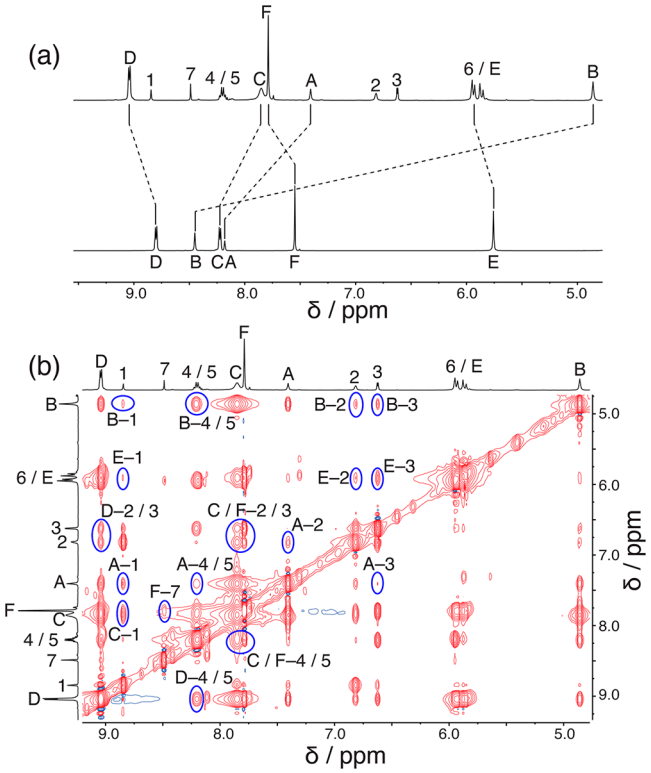

Figure 4. ^1H NMR spectroscopic investigation of the formation of the **Porp-2H⊂XCage^{8+}** complex. (a) ^1H NMR (500 MHz, D_2O, 25 °C) spectra of (top) the equilibrated **Porp-2H⊂XCage^{8+}** and (bottom) **XCage^{8+}**. (b) $^1H-^1H$ NOESY (500 MHz, D_2O, 25 °C, 0.2 s mixing time) of the equilibrated **Porp-2H⊂XCage^{8+}**. Proton labels are defined on the relevant structural formulas in Figure 1.

where the phenyl groups actually contribute to the overall stability of the complex by supporting several [CH···π] interactions with **XCage^{8+}**. While controlling the transformation of these two co-conformers is beyond the scope of this investigation, it is worth noting that this type of co-conformational isomerization could lead to new opportunities to manipulate multiple binding states within a multicyclic receptor.

The ^1H NMR spectrum of the equilibrated **Porp-2H⊂XCage^{8+}** in D_2O reveals (Figure 3) distinctive peaks for porphyrin units as co-conformer H.[61] Protons D, E, and F on **XCage^{8+}** experience the deshielding effect of the aromatic porphyrin ring and are downfield shifted. Protons A and C, which are positioned within the porphyrin shielding region, experience upfield shifts. Protons B, facing the shielding center of the porphyrin ring, experience the most dramatic upfield shift ($\Delta\delta = -3.6$ ppm). A NOESY experiment confirmed (Figure 4) the encapsulated structure by showing[62] the expected through-space correlation peaks between **Porp-2H** and **XCage^{8+}**. It is worthy of note that the triazole rings are also likely to participate in binding with **XCage^{8+}**, as revealed by the through-space correlations between the triazole ring protons 7 and protons F. Such a guest-backfolding phenomenon has been attributed[23,63,64] to stabilization of the complex by noncovalent bonding interactions. The corresponding ^1H NMR spectroscopic analysis of **Porp-Zn⊂XCage^{8+}** is described in the Supporting Information.

Photophysical Properties. The association between **Porp-2H(Zn)** and **XCage^{8+}** induces characteristic changes in the optical properties of the porphyrin moiety. Red-shifted absorption and emission (Figure 5a,b) of the encapsulated **Porp-2H** were observed, and its fluorescence quantum yield was enhanced from 16 to 25%, benefiting from the porphyrin being

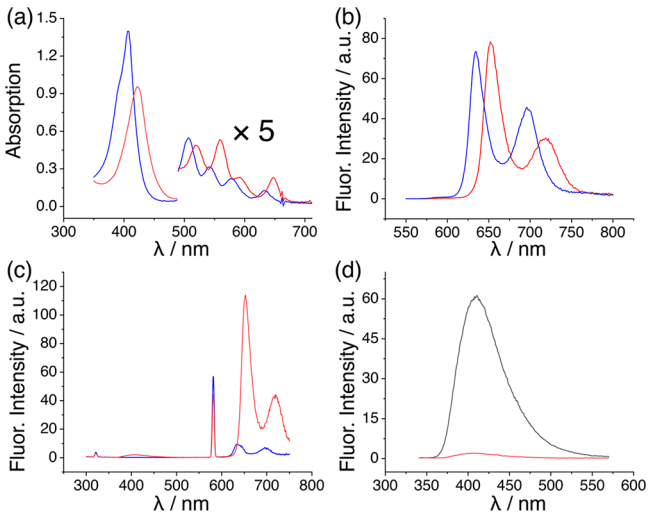

Figure 5. Steady-state absorption and emission spectra. (a) Absorption and (b) emission (ex: 440 nm) spectra of **Porp-2H** (blue, 10 μM) and **Porp-2H⊂XCage^{8+}** (red, 10 μM). (c) Emission spectra (ex: 290 nm) of **Porp-2H** (blue, 1 μM) and **Porp-2H⊂XCage^{8+}** (red, 1 μM). (d) Emission spectra (ex: 330 nm) of **XCage^{8+}** (black, 1 μM) and **Porp-2H⊂XCage^{8+}** (red, 1 μM). All spectra were collected in H_2O at 25 °C.

isolated in the hydrophobic binding pocket of **XCage^{8+}**. In comparison, previously reported porphyrin receptors either quench[57] the fluorescence or fail to induce any photophysical response.[55] The encapsulation of **Porp-Zn** by **XCage^{8+}** decreases the fluorescence quantum yield from 5 to 0.6%.

https://dx.doi.org/10.1021/jacs.0c02311
J. Am. Chem. Soc. 2020, 142, 8938−8945

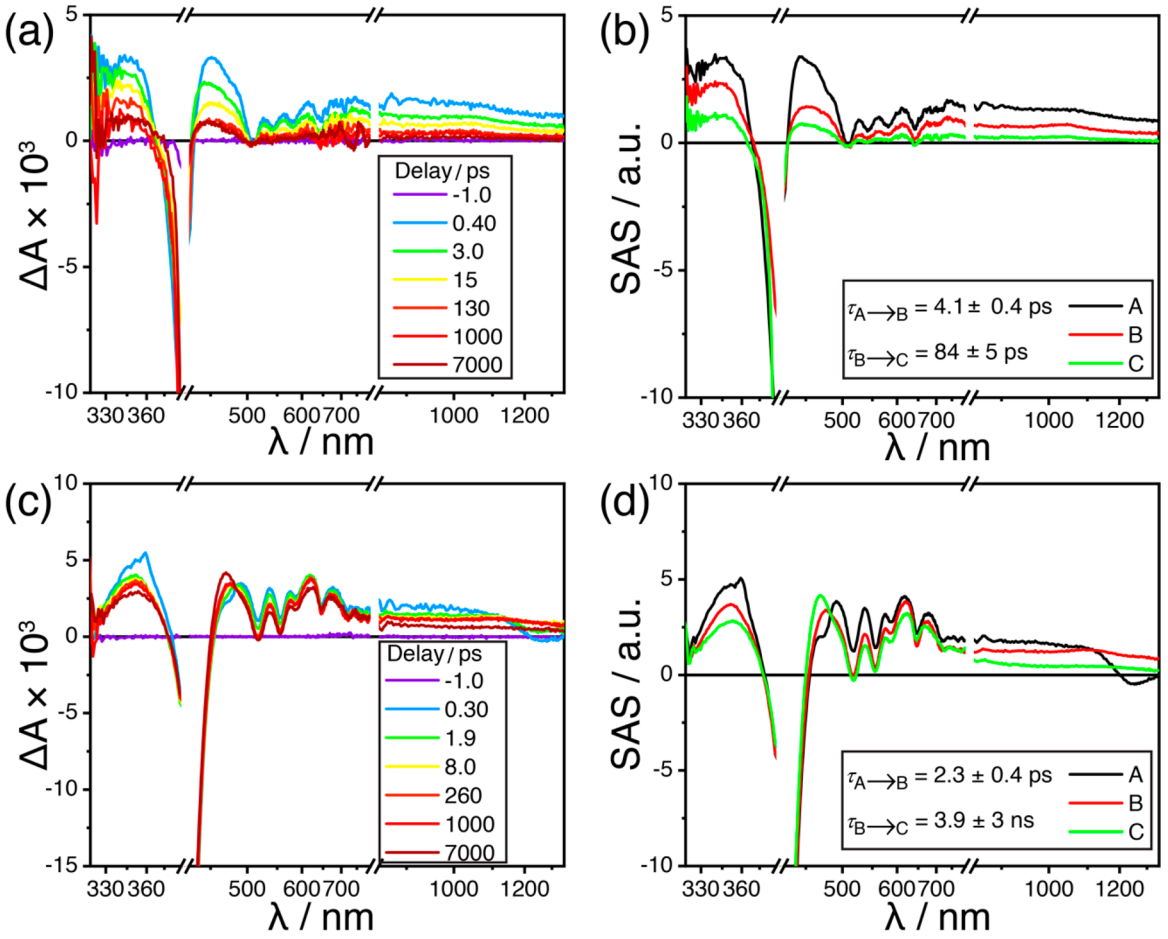

Figure 6. Femtosecond transient absorption spectroscopy. Femtosecond TA spectra of (a) **Porp-2H** and (c) **Porp-2H⊂XCage**$^{8+}$ in H_2O excited at 414 nm. Species-associated spectra of (b) **Porp-2H** and (d) **Porp-2H⊂XCage**$^{8+}$ obtained by wavelength global fitting to an A → B → C kinetic model. State A represents the higher singlet excited state S_2 ^{1}***Porp-2H**, state B is the lowest singlet excited state S_1 ^{1}***Porp-2H**, and state C is the triplet state T_1 ^{3}***Porp-2H**. State C in (d) is not fully resolved on account of the slow ISC rate.

Table 1. Binding Constants and Thermodynamic Data at 25 °C[a]

entry	host	guest	K_a[b]/M^{-1}	ΔG[c]/kcal mol^{-1}	ΔH[d]/kcal mol^{-1}	$T\Delta S$/kcal mol^{-1}
1	**ExBox**$^{4+}$	**Porp-2H**	1.4×10^7	−9.7	−7.7	+2.0
2	**ExBox**$^{4+}$	**Porp-Zn**	5.1×10^6	−9.1	−5.4	+3.7
3	**XCage**$^{8+}$	**Porp-2H**	1.7×10^{10}	−13.9	−16.1	−2.2
4	**XCage**$^{8+}$	**Porp-Zn**	6.2×10^9	−13.4	−12.8	+0.6

[a]The standard errors are presented in the Supporting Information. [b]Determined by fluorescence titration. [c]Estimated from fluorescence titration. [d]Measured by ITC.

There is an efficient energy transfer process from **XCage**$^{8+}$ to **Porp-2H**. When excited at 290 nm, the complex exhibits (Figure 5c) strong emission peaks for the **Porp-2H⊂XCage**$^{8+}$ complex at 650 nm. The energy transfer efficiency was estimated by comparing (Figure 5d) the fluorescence emission spectra of **XCage**$^{8+}$ and **Porp-2H⊂XCage**$^{8+}$ excited at 330 nm. The close-to-complete fluorescence quenching of **XCage**$^{8+}$ in the complex of **Porp-2H⊂XCage**$^{8+}$ is a compelling sign of the efficient energy transfer, which is calculated to be >96%. Time-dependent DFT calculations carried out on **Porp-2H⊂XCage**$^{8+}$ reveal that the HOMO is localized on **Porp-2H** and the LUMO on **XCage**$^{8+}$. The calculated UV−vis absorption spectrum of **Porp-2H⊂XCage**$^{8+}$ is red-shifted compared with that of **Porp-2H**, which is in agreement with experimental observations.

In order to gain a better understanding of the influence of molecular encapsulation on photophysical properties, transient absorption (TA) experiments were performed at femtosecond and nanosecond resolutions. Femtosecond TA studies, exciting the Soret band at 414 nm, reveal (Figure 6) a significant enhancement of the lifetime of intersystem crossing when **Porp-2H** is encapsulated in the cavity of **XCage**$^{8+}$. This result corroborates the enhanced fluorescence quantum yield of **Porp-2H⊂XCage**$^{8+}$. Compared to **Porp-2H**, **Porp-2H⊂XCage**$^{8+}$ shows improved stability of the triplet state as revealed by the nanosecond TA spectra (see Figures S34 and S38). The energy transfer within **Porp-2H⊂XCage**$^{8+}$ was investigated by femtosecond TA spectroscopy using an excitation wavelength of 330 nm. Under these conditions, we only observed (Figure S43) the excited state of **Porp-2H**, and no excited state of **XCage**$^{8+}$ could be detected (Figure S41) within 0.4 ps, suggesting an ultrafast rate of energy transfer, which corroborate the efficient energy transfer process observed by the fluorescence emission spec-

https://dx.doi.org/10.1021/jacs.0c02311
J. Am. Chem. Soc. 2020, 142, 8938−8945

troscopy. In contrast to **Porp-2H⊂XCage**$^{8+}$, femtosecond TA spectra (Figure S39) of **Porp-Zn⊂XCage**$^{8+}$ shows a charge-separated state, accounting for the decreased fluorescence of this complex.

Binding Thermodynamics and Kinetics. The changes in optical properties upon porphyrin encapsulation enable a facile study of the binding events. Fluorescence titrations of **Porp-2H** and **Porp-Zn** with **ExBox**$^{4+}$ yielded directly their binding constants in water. Since the binding affinities for **XCage**$^{8+}$ with **Porp-2H** and **Porp-Zn** are too high to be determined directly, competitive titrations were performed by displacing **ExBox**$^{4+}$ with **XCage**$^{8+}$ from the complex **Porp-2H(Zn)⊂ExBox**$^{4+}$. The binding affinities (Table 1) between **ExBox**$^{4+}$ and the two porphyrins are on the order of 10^7 M^{-1}. Compared with **ExBox**$^{4+}$, **XCage**$^{8+}$ shows around a 1000-fold enhancement in the binding affinities, which are around 10^{10} M^{-1} (K_d = 0.1 nM). The highest affinity ($K_a = 1.7 \times 10^{10}$ M^{-1}) was achieved in the binding between **XCage**$^{8+}$ and **Porp-2H**. It should be noted that these K_a values are interpreted as a lower limit to the stability constant, as the measurement was performed under conditions where co-conformers V and H coexist[65] in solution. The equilibrated co-conformer H is expected to have a higher stability with the absence of the metastable species.

Since the high binding affinity and aggregation of the two porphyrins prevent the accurate measurement of binding constants by isothermal titration calorimetry (ITC), a single injection experiment was performed in order to determine the binding enthalpy. The Gibbs free energy of the receptor–substrate complexation was estimated directly from the corresponding fluorescent titrations, providing a value for $T\Delta S$. Compared with **ExBox**$^{4+}$, the binding enthalpies of **XCage**$^{8+}$ are in the range of 7–8 kcal mol^{-1} larger, a major contributing factor to the enhanced affinity. Surface area overlap analysis reveals[66] that **XCage**$^{8+}$ provides 1.5 times more binding surface area for the porphyrin core compared with that of **ExBox**$^{4+}$: 80% of the porphyrin core overlaps with **XCage**$^{8+}$, whereas only 50% of the porphyrin core overlaps in the case of **ExBox**$^{4+}$. Compared with **Porp-2H**, **Porp-Zn** shows a significant drop in binding enthalpy toward both **XCage**$^{8+}$ and **ExBox**$^{4+}$, an observation that agrees well with the titration results which show that the binding of **Porp-Zn** is generally 3 times weaker compared with that of **Porp-2H**. This result implies that the dehydration of the Zn ion upon binding is an energy-demanding process.

The kinetics of porphyrin encapsulation by **XCage**$^{8+}$ can be tracked by the change in fluorescence over time. The resulting kinetic profiles were fitted (Figures S53 and S54) using a second-order kinetics equation. The threading rate constants of **XCage**$^{8+}$ with **Porp-2H** and **Porp-Zn** were determined[67] to be 7.2×10^4 and 4.6×10^4 M^{-1} s^{-1}, respectively. The remarkably rapid threading kinetics agrees well with previously reported[24] results where threading a long polymer chain through a macrocyclic receptor is a rapid process. It is necessary to note that the rapid threading kinetics measured here represent the formation of the **Porp-2H(Zn)⊂XCage**$^{8+}$ complexes, in which co-conformers V and H coexist as a mixture. The transformation of co-conformer V into H is a slow process and requires days to reach completion. Furthermore, the slower threading kinetics of **Porp-Zn** matches well with the observed co-conformer distribution, where a lesser amount of the metastable co-conformer V is formed when compared with **Porp-2H**. The dissociation rate constants (k_{off}) for the **Porp-2H(Zn)⊂XCage**$^{8+}$ complexes can be calculated using the equation $k_{off} = k_{on}/K_a$, which reveals extremely slow dissociation processes with the rate constants and half-lives ($t_{1/2}$) calculated at 4.2×10^{-6} ($t_{1/2}$ = 46 h) and 7.4×10^{-6} s^{-1} ($t_{1/2}$ = 26 h) for **Porp-2H⊂XCage**$^{8+}$ and **Porp-Zn⊂XCage**$^{8+}$, respectively. The slow dissociations of **Porp-2H(Zn)⊂XCage**$^{8+}$ endow the complexes with kinetic stabilities, wherein considerable amounts of the 1:1 complexes can still exist for days, even in the presence of a competitor that has a stronger binding affinity with **XCage**$^{8+}$.

Chemical Stability. It is well known that porphyrins and metalloporphyrin are susceptible to acidic environments. Protonation occurs at the pyrrole subunits and leads to changes in photophysical properties which limit their performance in certain technical scenarios. When added to a solution of HCl (1 M), **Porp-2H** is protonated instantly, as judged from the change of its color from brown to green and a red-shifted absorption in the UV–vis spectrum (Figure 7a). In contrast, **Porp-2H⊂XCage**$^{8+}$ resists protonation, and no change is observed (Figure 7b) under the same conditions; i.e., the high charge density of **XCage**$^{8+}$ plus its strong affinity with **Porp-2H** provide protection from H^+ attack in aqueous solution. Encapsulation-facilitated protonation (positive pK_a shifts) is well documented,[68−71] whereas examples of frustrated protonation (negative pK_a shifts), induced by synthetic receptors, are rare.[72] There is no example, to our knowledge, where protonation can be totally shut down by molecular encapsulation, a property which would require a high binding affinity and the protection of the protonation site deep inside the binding cavity. As a comparison, the **Porp-2H⊂ExBox**$^{4+}$ complex, with four positive charges and a micromolar binding affinity, fails to provide these kinds of protection and instantly dissociates (Figure S60) into the corresponding protonated species, namely **Porp-4H**$^{2+}$ and **ExBox**$^{4+}$, under the same conditions. On the other hand, **Porp-Zn** suffers (Figure S59) from solvolysis in the presence of HCl (1 M) as judged by the appearance of **Porp-4H**$^{2+}$ in its absorption spectrum. **Porp-Zn⊂XCage**$^{8+}$ remains stable in HCl solution.

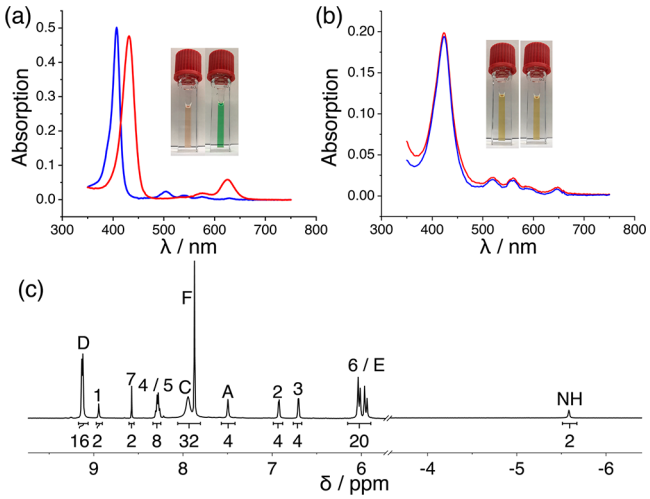

Figure 7. Stability test of **Porp-2H** and **Porp-2H⊂XCage**$^{8+}$. Absorption spectra of (a) **Porp-2H** and (b) **Porp-2H⊂XCage**$^{8+}$ in H_2O (blue) and 1 M HCl (red). Insets show the corresponding solutions in H_2O (left) and HCl (right). (c) ^1H NMR (500 MHz, D_2O, 25 °C) spectrum of the pre-assembled **Porp-2H⊂XCage**$^{8+}$ in D_2O.

Considering the excellent performance of **XCage**$^{8+}$ which prevents H^+ from attacking the porphyrin core, we envisioned that D/H exchanges, involving the pyrrole subunits in

https://dx.doi.org/10.1021/jacs.0c02311
J. Am. Chem. Soc. 2020, 142, 8938−8945

deuterated solvents, should also be blocked. In order to test this hypothesis, **Porp-2H⊂XCage**$^{8+}$ was prepared, first of all in H_2O, and subsequently redissolved in D_2O. The ^{1}H NMR spectrum of **Porp-2H⊂XCage**$^{8+}$ shows (Figure 7c) clearly NH signals at −5.6 ppm, resulting from the shielding effect provided by both the porphyrin core and the biphenyl units in **XCage**$^{8+}$. A comparison of the NH integration, with respect to other porphyrin proton signals, indicates[73] no sign of D/H exchange.

CONCLUSIONS

The tricyclic cyclophane serves as an excellent receptor for both the free-base and Zn-porphyrins with subnanomolar affinity in water. The tricyclic nature of **XCage**$^{8+}$ permits the formation of two co-conformationally isomeric complexes with both porphyrins, as revealed by ^{1}H NMR spectroscopy. **XCage**$^{8+}$ is able to modulate both the photophysical properties and chemical reactivities of the encapsulated porphyrins. The isolation of both porphyrins by **XCage**$^{8+}$ with ultrahigh stabilities provides us with a new platform to investigate porphyrins at the single-molecule level.[74−76] We speculate that the encapsulation characterizing the **Porp-Zn⊂XCage**$^{8+}$ complex could be quite general for a library of metalloporphyrins with a wide range of properties, leading to applications in nanotechnology,[43,77] artificial photodevice fabrication,[78,79] and biomedical science.[41,80]

ASSOCIATED CONTENT

Supporting Information

The Supporting Information is available free of charge at https://pubs.acs.org/doi/10.1021/jacs.0c02311.

Experimental procedures, chemical synthesis and characterization, mass spectral data, NMR spectra, X-ray crystal data, computational analysis, photophysical data, binding studies, and chemical stability studies, including Figures S1−S62 and Tables S1 and S2 (PDF)

Crystallographic data for **mPorp-2H⊂XCage**·8PF_6 (CIF)

Crystallographic data for **mPorp-Zn⊂XCage**·8PF_6 (CIF)

AUTHOR INFORMATION

Corresponding Author

J. Fraser Stoddart − *Department of Chemistry, Northwestern University, Evanston, Illinois 60208, United States; Institute for Molecular Design and Synthesis, Tianjin University, Tianjin 300072, China; School of Chemistry, University of New South Wales, Sydney, NSW 2052, Australia;* orcid.org/0000-0003-3161-3697; Email: stoddart@northwestern.edu

Authors

Wenqi Liu − *Department of Chemistry, Northwestern University, Evanston, Illinois 60208, United States;* orcid.org/0000-0001-6408-0204

Chenjian Lin − *Department of Chemistry, Northwestern University, Evanston, Illinois 60208, United States;* orcid.org/0000-0002-8817-5133

Jacob A. Weber − *Department of Chemistry, Northwestern University, Evanston, Illinois 60208, United States*

Charlotte L. Stern − *Department of Chemistry, Northwestern University, Evanston, Illinois 60208, United States*

Ryan M. Young − *Department of Chemistry, Northwestern University, Evanston, Illinois 60208, United States;* orcid.org/0000-0002-5108-0261

Michael R. Wasielewski − *Department of Chemistry, Northwestern University, Evanston, Illinois 60208, United States;* orcid.org/0000-0003-2920-5440

Complete contact information is available at: https://pubs.acs.org/10.1021/jacs.0c02311

Notes

The authors declare no competing financial interest.

ACKNOWLEDGMENTS

We thank Northwestern University (NU) for their support of this research. We also thank the personnel in the Integrated Molecular Structure Education and Research Center (IMSERC) at NU for their assistance in the collection of the data. This project was supported in the Wasielewski laboratory by the National Science Foundation under grant number DMR-1710104 (M.R.W.).

REFERENCES

(1) Persch, E.; Dumele, O.; Diederich, F. Molecular Recognition in Chemical and Biological Systems. *Angew. Chem., Int. Ed.* **2015**, *54*, 3290−3327.

(2) Houk, K. N.; Leach, A. G.; Kim, S. P.; Zhang, X. Binding Affinities of Host-Guest, Protein-Ligand, and Protein-Transition-State Complexes. *Angew. Chem., Int. Ed.* **2003**, *42*, 4872−4897.

(3) *Synthetic Receptors for Biomolecules: Design Principles and Applications*, 1st ed.; Smith, B. D., Ed.; Royal Society of Chemistry, 2015.

(4) Liu, W.; Samanta, S. K.; Smith, B. D.; Isaacs, L. Synthetic Mimics of Biotin/(Strept)Avidin. *Chem. Soc. Rev.* **2017**, *46*, 2391−2403.

(5) Cao, L.; Šekutor, M.; Zavalij, P. Y.; Mlinarić-Majerski, K.; Glaser, R.; Isaacs, L. Cucurbit[7]uril·Guest Pair with an Attomolar Dissociation Constant. *Angew. Chem., Int. Ed.* **2014**, *53*, 988−993.

(6) Tromans, R. A.; Carter, T. S.; Chabanne, L.; Crump, M. P.; Li, H.; Matlock, J. V.; Orchard, M. G.; Davis, A. P. A Biomimetic Receptor for Glucose. *Nat. Chem.* **2019**, *11*, 52−56.

(7) Shetty, D.; Khedkar, J. K.; Park, K. M.; Kim, K. Can We Beat the Biotin-Avidin Pair?: Cucurbit[7]uril-Based Ultrahigh Affinity Host-Guest Complexes and Their Applications. *Chem. Soc. Rev.* **2015**, *44*, 8747−8761.

(8) Mako, T. L.; Racicot, J. M.; Levine, M. Supramolecular Luminescent Sensors. *Chem. Rev.* **2019**, *119*, 322−477.

(9) Jia, F.; Hupatz, H.; Yang, L. P.; Schröder, H. V.; Li, D. H.; Xin, S.; Lentz, D.; Witte, F.; Xie, X.; Paulus, B.; Schalley, C. A.; Jiang, W. Naphthocage: A Flexible yet Extremely Strong Binder for Singly Charged Organic Cations. *J. Am. Chem. Soc.* **2019**, *141*, 4468−4473.

(10) Cheng, C.; McGonigal, P. R.; Schneebeli, S. T.; Li, H.; Vermeulen, N. A.; Ke, C.; Stoddart, J. F. An Artificial Molecular Pump. *Nat. Nanotechnol.* **2015**, *10*, 547−553.

(11) Qiu, Y.; Zhang, L.; Pezzato, C.; Feng, Y.; Li, W.; Nguyen, M. T.; Cheng, C.; Shen, D.; Guo, Q. H.; Shi, Y.; Cai, K.; Alsubaie, F. M.; Astumian, R. D.; Stoddart, J. F. A Molecular Dual Pump. *J. Am. Chem. Soc.* **2019**, *141*, 17472−17476.

(12) Yoshizawa, M.; Catti, L. Bent Anthracene Dimers as Versatile Building Blocks for Supramolecular Capsules. *Acc. Chem. Res.* **2019**, *52*, 2392−2404.

(13) Yazaki, K.; Catti, L.; Yoshizawa, M. Polyaromatic Molecular Tubes: From Strategic Synthesis to Host Functions. *Chem. Commun.* **2018**, *54*, 3195−3206.

(14) Yang, L. P.; Wang, X.; Yao, H.; Jiang, W. Naphthotubes: Macrocyclic Hosts with a Biomimetic Cavity Feature. *Acc. Chem. Res.* **2020**, *53*, 198−208.

(15) Ke, H.; Yang, L.-P.; Xie, M.; Chen, Z.; Yao, H.; Jiang, W. Shear-Induced Assembly of a Transient yet Highly Stretchable Hydrogel Based on Pseudopolyrotaxanes. *Nat. Chem.* **2019**, *11*, 470−477.

(16) Yamashina, M.; Sartin, M. M.; Sei, Y.; Akita, M.; Takeuchi, S.; Tahara, T.; Yoshizawa, M. Preparation of Highly Fluorescent Host-

Guest Complexes with Tunable Color Upon Encapsulation. *J. Am. Chem. Soc.* **2015**, *137*, 9266−9269.
(17) Hagiwara, K.; Akita, M.; Yoshizawa, M. An Aqueous Molecular Tube with Polyaromatic Frameworks Capable of Binding Fluorescent Dyes. *Chem. Sci.* **2015**, *6*, 259−263.
(18) Kondo, K.; Akita, M.; Yoshizawa, M. Solubility Switching of Metallophthalocyanines and Their Larger Derivatives upon Encapsulation. *Chem. - Eur. J.* **2016**, *22*, 1937−1940.
(19) Tsutsui, T.; Kusaba, S.; Yamashina, M.; Akita, M.; Yoshizawa, M. Open Versus Closed Polyaromatic Nanocavity: Enhanced Host Abilities toward Large Dyes and Pigments. *Chem. - Eur. J.* **2019**, *25*, 4320−4324.
(20) Arunkumar, E.; Forbes, C. C.; Smith, B. D. Improving the Properties of Organic Dyes by Molecular Encapsulation. *Eur. J. Org. Chem.* **2005**, *19*, 4051−4059.
(21) Koner, A. L.; Nau, W. M. Cucurbituril Encapsulation of Fluorescent Dyes. *Supramol. Chem.* **2007**, *19*, 55−66.
(22) Dsouza, R. N.; Pischel, U.; Nau, W. M. Fluorescent Dyes and Their Supramolecular Host/Guest Complexes with Macrocycles in Aqueous Solution. *Chem. Rev.* **2011**, *111*, 7941−7980.
(23) Liu, W.; Johnson, A.; Smith, B. D. Guest Back-Folding: A Molecular Design Strategy That Produces a Deep-Red Fluorescent Host/Guest Pair with Picomolar Affinity in Water. *J. Am. Chem. Soc.* **2018**, *140*, 3361−3370.
(24) Peck, E. M.; Liu, W.; Spence, G. T.; Shaw, S. K.; Davis, A. P.; Destecroix, H.; Smith, B. D. Rapid Macrocycle Threading by a Fluorescent Dye-Polymer Conjugate in Water with Nanomolar Affinity. *J. Am. Chem. Soc.* **2015**, *137*, 8668−8671.
(25) Liu, W.; Peck, E. M.; Smith, B. D. High Affinity Macrocycle Threading by a Near-Infrared Croconaine Dye with Flanking Polymer Chains. *J. Phys. Chem. B* **2016**, *120*, 995−1001.
(26) Mohanty, J.; Nau, W. M. Ultrastable Rhodamine with Cucurbituril. *Angew. Chem., Int. Ed.* **2005**, *44*, 3750−3754.
(27) Liu, W.; Bobbala, S.; Stern, C. L.; Hornick, J. E.; Liu, Y.; Enciso, A. E.; Scott, E. A.; Stoddart, J. F. XCage: A Tricyclic Octacationic Receptor for Perylene Diimide with Picomolar Affinity in Water. *J. Am. Chem. Soc.* **2020**, *142*, 3165−3173.
(28) Schreiber, C. L.; Smith, B. D. Molecular Conjugation Using Non-Covalent Click Chemistry. *Nat. Rev. Chem.* **2019**, *3*, 393−400.
(29) Milgrom, L. R. *The Colours of Life: An Introduction to the Chemistry of Porphyrins and Related Compounds*; Oxford University Press: Oxford, New York, Tokyo, 1997.
(30) Lombardi, A.; Nastri, F.; Pavone, V. Peptide-Based Heme-Protein Models. *Chem. Rev.* **2001**, *101*, 3165−3189.
(31) Reedy, C. J.; Gibney, B. R. Heme Protein Assemblies. *Chem. Rev.* **2004**, *104*, 617−649.
(32) Bols, P. S.; Anderson, H. L. Template-Directed Synthesis of Molecular Nanorings and Cages. *Acc. Chem. Res.* **2018**, *51*, 2083−2092.
(33) Yim, D.; Sung, J.; Kim, S.; Oh, J.; Yoon, H.; Sung, Y. M.; Kim, D.; Jang, W.-D. Guest-Induced Modulation of the Energy Transfer Process in Porphyrin-Based Artificial Light Harvesting Dendrimers. *J. Am. Chem. Soc.* **2017**, *139*, 993−1002.
(34) Liu, Y.; Jin, J.; Deng, H.; Li, K.; Zheng, Y.; Yu, C.; Zhou, Y. Protein-Framed Multi-Porphyrin Micelles for a Hybrid Natural-Artificial Light-Harvesting Nanosystem. *Angew. Chem., Int. Ed.* **2016**, *55*, 7952−7957.
(35) Omagari, T.; Suzuki, A.; Akita, M.; Yoshizawa, M. Efficient Catalytic Epoxidation in Water by Axial *N*-Ligand-Free Mn-Porphyrins within a Micellar Capsule. *J. Am. Chem. Soc.* **2016**, *138*, 499−502.
(36) Adam, S. M.; Wijeratne, G. B.; Rogler, P. J.; Diaz, D. E.; Quist, D. A.; Liu, J. J.; Karlin, K. D. Synthetic Fe/Cu Complexes: Toward Understanding Heme-Copper Oxidase Structure and Function. *Chem. Rev.* **2018**, *118*, 10840−11022.
(37) Kitagishi, H.; Tamaki, M.; Ueda, T.; Hirota, S.; Ohta, T.; Naruta, Y.; Kano, K. Oxoferryl Porphyrin/Hydrogen Peroxide System Whose Behavior Is Equivalent to Hydroperoxoferric Porphyrin. *J. Am. Chem. Soc.* **2010**, *132*, 16730−16732.
(38) Kano, K.; Kitagishi, H.; Kodera, M.; Hirota, S. Dioxygen Binding to a Simple Myoglobin Model in Aqueous Solution. *Angew. Chem., Int. Ed.* **2005**, *44*, 435−438.
(39) Merlau, M. L.; Mejia, M. D. P.; Nguyen, S. T.; Hupp, J. T. Artificial Enzymes Formed through Directed Assembly of Molecular Square Encapsulated Epoxidation Catalysts. *Angew. Chem., Int. Ed.* **2001**, *40*, 4239−4242.
(40) Elemans, J. A. A. W.; Nolte, R. J. M. Porphyrin Cage Compounds Based on Glycoluril − from Enzyme Mimics to Functional Molecular Machines. *Chem. Commun.* **2019**, *55*, 9590−9605.
(41) Rajora, M. A.; Lou, J. W. H.; Zheng, G. Advancing Porphyrin's Biomedical Utility *via* Supramolecular Chemistry. *Chem. Soc. Rev.* **2017**, *46*, 6433−6469.
(42) Ethirajan, M.; Chen, Y.; Joshi, P.; Pandey, R. K. The Role of Porphyrin Chemistry in Tumor Imaging and Photodynamic Therapy. *Chem. Soc. Rev.* **2011**, *40*, 340−362.
(43) Kundu, S.; Patra, A. Nanoscale Strategies for Light Harvesting. *Chem. Rev.* **2017**, *117*, 712−757.
(44) Galan, A.; Ballester, P. Stabilization of Reactive Species by Supramolecular Encapsulation. *Chem. Soc. Rev.* **2016**, *45*, 1720−1737.
(45) Polizzi, N. F.; Wu, Y.; Lemmin, T.; Maxwell, A. M.; Zhang, S. Q.; Rawson, J.; Beratan, D. N.; Therien, M. J.; DeGrado, W. F. De Novo Design of a Hyperstable Non-Natural Protein-Ligand Complex with Sub-Å Accuracy. *Nat. Chem.* **2017**, *9*, 1157−1164.
(46) Qi, Q.; Yang, C.; Xia, Y.; Guo, S.; Song, D.; Su, H. Preferential Binding of π-Ligand Porphyrin Targeting 5′-5′ Stacking Interface of Human Telomeric RNA G-Quadruplex Dimer. *J. Phys. Chem. Lett.* **2019**, *10*, 2143−2150.
(47) Börjesson, K.; Wiberg, J.; El-Sagheer, A. H.; Ljungdahl, T.; Mårtensson, J.; Brown, T.; Nordén, B.; Albinsson, B. Functionalized Nanostructures: Redox-Active Porphyrin Anchors for Supramolecular DNA Assemblies. *ACS Nano* **2010**, *4*, 5037−5046.
(48) Goto, Y.; Sugikawa, K.; Ikeda, A. Enhancement in Guest Molecule Incorporation into Lipid Membranes in the Presence of Zinc-Porphyrin Anchor Molecules. *ChemistrySelect* **2019**, *4*, 134−137.
(49) Synytsya, A.; Synytsya, A.; Blafkova, P.; Volka, K.; Král, V. Interaction of *meso*-Tetrakis(4-sulphonatophenyl)porphine with Chitosan in Aqueous Solutions. *Spectrochim. Acta, Part A* **2007**, *66*, 225−235.
(50) Venema, F.; Rowan, A. E.; Nolte, R. J. M. Binding of Porphyrins in Cyclodextrin Dimers. *J. Am. Chem. Soc.* **1996**, *118*, 257−258.
(51) Pathak, P.; Yao, W.; Hook, K. D.; Vik, R.; Winnerdy, F. R.; Brown, J. Q.; Gibb, B. C.; Pursell, Z. F.; Phan, A. T.; Jayawickramarajah, J. Bright G-Quadruplex Nanostructures Functionalized with Porphyrin Lanterns. *J. Am. Chem. Soc.* **2019**, *141*, 12582−12591.
(52) Watanabe, K.; Kitagishi, H.; Kano, K. Supramolecular Iron Porphyrin/Cyclodextrin Dimer Complex that Mimics the Functions of Hemoglobin and Methemoglobin. *Angew. Chem., Int. Ed.* **2013**, *52*, 6894−6897.
(53) Moschetto, G.; Lauceri, R.; Gulino, F. G.; Sciotto, D.; Purrello, R. Non-Covalent Synthesis in Aqueous Solution of Discrete Multi-Porphyrin Aggregates with Programmable Stoichiometry and Sequence. *J. Am. Chem. Soc.* **2002**, *124*, 14536−14537.
(54) Kubota, R.; Takabe, T.; Arima, K.; Taniguchi, H.; Asayama, S.; Kawakami, H. New Class of Artificial Enzyme Composed of Mn-Porphyrin, Imidazole, and Cucurbit[10]Uril toward Use as a Therapeutic Antioxidant. *J. Mater. Chem. B* **2018**, *6*, 7050−7059.
(55) Liu, S.; Shukla, A. D.; Gadde, S.; Wagner, B. D.; Kaifer, A. E.; Isaacs, L. Ternary Complexes Comprising Cucurbit[10]uril, Porphyrins, and Guests. *Angew. Chem., Int. Ed.* **2008**, *47*, 2657−2660.
(56) Juríček, M.; Barnes, J. C.; Strutt, N. L.; Vermeulen, N. A.; Ghooray, K. C.; Dale, E. J.; McGonigal, P. R.; Blackburn, A. K.; Avestro, A.-J.; Stoddart, J. F. An ExBox [2]Catenane. *Chem. Sci.* **2014**, *5*, 2724.
(57) Roy, I.; Bobbala, S.; Young, R. M.; Beldjoudi, Y.; Nguyen, M. T.; Cetin, M. M.; Cooper, J. A.; Allen, S.; Anamimoghadam, O.; Scott, E. A.; Wasielewski, M. R.; Stoddart, J. F. A Supramolecular Approach for Modulated Photoprotection, Lysosomal Delivery, and Photodynamic Activity of a Photosensitizer. *J. Am. Chem. Soc.* **2019**, *141*, 12296−12304.

https://dx.doi.org/10.1021/jacs.0c02311
J. Am. Chem. Soc. 2020, 142, 8938−8945

(58) Wu, Z. Q.; Li, C. Z.; Feng, D. J.; Jiang, X. K.; Li, Z. T. Foldamer-Based Pyridine-Fullerene Tweezer Receptors for Enhanced Binding of Zinc Porphyrin. *Tetrahedron* **2006**, *62*, 11054−11062.
(59) Ono, K.; Yoshizawa, M.; Kato, T.; Watanabe, K.; Fujita, M. Porphine Dimeric Assemblies in Organic-Pillared Coordination Cages. *Angew. Chem., Int. Ed.* **2007**, *46*, 1803−1806.
(60) Lefebvre, C.; Rubez, G.; Khartabil, H.; Boisson, J. C.; Contreras-García, J.; Hénon, E. Accurately Extracting the Signature of Intermolecular Interactions Present in the NCI Plot of the Reduced Density Gradient *versus* Electron Density. *Phys. Chem. Chem. Phys.* **2017**, *19*, 17928−17936.
(61) The amphiphilic nature of **Porp-2H** and **Porp-Zn** leads to their aggregation in D_2O, causing the proton resonances in prophyrins to be masked.
(62) Since no NOE signal is observed between the long PEG chians and **XCage**$^{8+}$, these chains do not contribute to the overall stability of the complexes.
(63) Dempsey, J. M.; Zhai, C.; McGarraugh, H. H.; Schreiber, C. L.; Stoffel, S. E.; Johnson, A.; Smith, B. D. High Affinity Threading of a New Tetralactam Macrocycle in Water by Fluorescent Deep-Red and near-Infrared Squaraine Dyes. *Chem. Commun.* **2019**, *55*, 12793−12796.
(64) Cheng, C.; Cheng, T.; Xiao, H.; Krzyaniak, M. D.; Wang, Y.; McGonigal, P. R.; Frasconi, M.; Barnes, J. C.; Fahrenbach, A. C.; Wasielewski, M. R.; Goddard III, W. A.; Stoddart, J. F. Influence of Constitution and Charge on Radical Pairing Interactions in Tris-Radical Tricationic Complexes. *J. Am. Chem. Soc.* **2016**, *138*, 8288−8300.
(65) The samples were equilibrated for 6 h prior to the fluorescence titration studies. Based on time-dependent ^{1}H NMR spectroscopic experiments, the tranformation of co-conformer V to H requires 72 h or longer to reach completion.
(66) Dale, E. J.; Vermeulen, N. A.; Thomas, A. A.; Barnes, J. C.; Juríček, M.; Blackburn, A. K.; Strutt, N. L.; Sarjeant, A. A.; Stern, C. L.; Denmark, S. E.; Stoddart, J. F. ExCage. *J. Am. Chem. Soc.* **2014**, *136*, 10669−10682.
(67) The threading of **ExBox**$^{4+}$ is so rapid that no change of fluorescence over time could be detected following mixing of the tetracationic cyclophane with the porphyrins.
(68) Ghosh, I.; Nau, W. M. The Strategic Use of Supramolecular pK_a Shifts to Enhance the Bioavailability of Drugs. *Adv. Drug Delivery Rev.* **2012**, *64*, 764−783.
(69) Pluth, M. D.; Bergman, R. G.; Raymond, K. N. Making Amines Strong Bases: Thermodynamic Stabilization of Protonated Guests in a Highly-Charged Supramolecular Host. *J. Am. Chem. Soc.* **2007**, *129*, 11459−11467.
(70) Saleh, N.; Koner, A. L.; Nau, W. M. Activation and Stabilization of Drugs by Supramolecular pK_a Shifts: Drug-Delivery Applications Tailored for Cucurbiturils. *Angew. Chem., Int. Ed.* **2008**, *47*, 5398−5401.
(71) Wolter, A. C.; Weickhmann, A. K.; Nasiri, A. H.; Hantke, K.; Ohlenschläger, O.; Wunderlich, C. H.; Kreutz, C.; Duchardt-Ferner, E.; Wöhnert, J. A Stably Protonated Adenine Nucleotide with a Highly Shifted pK_aValue Stabilizes the Tertiary Structure of a GTP-Binding RNA Aptamer. *Angew. Chem., Int. Ed.* **2017**, *56*, 401−404.
(72) Yin, H.; Cheng, Q.; Rosas, R.; Viel, S.; Monnier, V.; Charles, L.; Siri, D.; Gigmes, D.; Ouari, O.; Wang, R.; Kermagoret, A.; Bardelang, D. A Cucurbit[8]uril 2:2 Complex with a Negative pK_a Shift. *Chem. - Eur. J.* **2019**, *25*, 12552−12559.
(73) A control study was performed using **Porp-2H** which was dissolved in CD_3OD. We found (Figure S62) that more than 99.9% of the NH signal at −3.2 ppm undergoes exchange to ND.
(74) Sedghi, G.; Sawada, K.; Esdaile, L. J.; Hoffmann, M.; Anderson, H. L.; Bethell, D.; Haiss, W.; Higgins, S. J.; Nichols, R. J. Single Molecule Conductance of Porphyrin Wires with Ultralow Attenuation. *J. Am. Chem. Soc.* **2008**, *130*, 8582−8583.
(75) Li, Z.; Borguet, E. Determining Charge Transport Pathways through Single Porphyrin Molecules Using Scanning Tunneling Microscopy Break Junctions. *J. Am. Chem. Soc.* **2012**, *134*, 63−66.
(76) Zhu, S. E.; Kuang, Y. M.; Geng, F.; Zhu, J. Z.; Wang, C. Z.; Yu, Y. J.; Luo, Y.; Xiao, Y.; Liu, K. Q.; Meng, Q. S.; Zhang, L.; Jiang, S.; Zhang, Y.; Wang, G. W.; Dong, Z. C.; Hou, J. G. Self-Decoupled Porphyrin with a Tripodal Anchor for Molecular-Scale Electroluminescence. *J. Am. Chem. Soc.* **2013**, *135*, 15794−15800.
(77) Wang, A.; Ye, J.; Humphrey, M. G.; Zhang, C. Graphene and Carbon-Nanotube Nanohybrids Covalently Functionalized by Porphyrins and Phthalocyanines for Optoelectronic Properties. *Adv. Mater.* **2018**, *30*, 1870118.
(78) Kesters, J.; Verstappen, P.; Kelchtermans, M.; Lutsen, L.; Vanderzande, D.; Maes, W. Porphyrin-Based Bulk Heterojunction Organic Photovoltaics: The Rise of the Colors of Life. *Adv. Energy Mater.* **2015**, *5*, 1500218.
(79) Otsuki, J. Supramolecular Approach towards Light-Harvesting Materials Based on Porphyrins and Chlorophylls. *J. Mater. Chem. A* **2018**, *6*, 6710−6753.
(80) Xue, X.; Lindstrom, A.; Li, Y. Porphyrin-Based Nanomedicines for Cancer Treatment. *Bioconjugate Chem.* **2019**, *30*, 1585−1603.

https://dx.doi.org/10.1021/jacs.0c02311
J. Am. Chem. Soc. 2020, 142, 8938−8945